Reinterpreting Space, Time Lags, and Functional Responses in Ecological Models

Matt J. Keeling *et al.*

Science **290**, 1758 (2000);
DOI: 10.1126/science.290.5497.1758

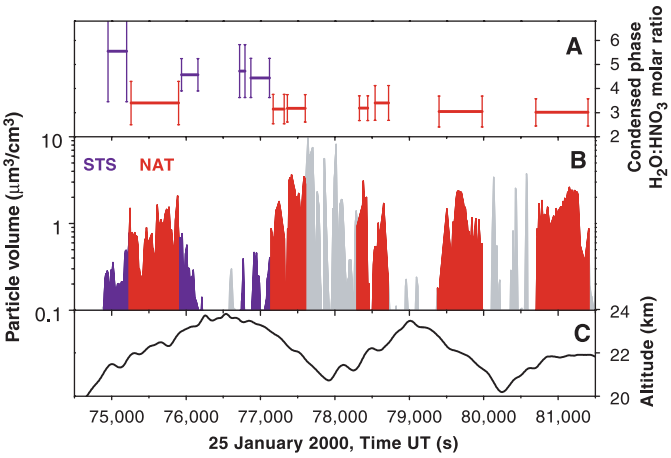

Fig. 3. Measured molar ratios (H_2O:HNO_3) of PSCs (**A**), together with the total particle volume in 1 cm^3 of air (**B**) and the altitude of the gondola (**C**) for reference. During the first ascent, the presence of STS particles is supported by low depolarization ratios (first and second blue areas, Fig. 2D) and of NAT particles by higher ratios near 75,500 s UT. During the periods marked as gray areas in (B), particles were detected by the ACMS; counting statistics, however, were not sufficient to derive molar ratios.

ferent in the north, where low-temperature periods are shorter and the vortex is less stable (*29, 30*). The question has been raised as to whether NAT particles can form in such an environment, although measurements have shown layers of liquid and solid aerosols at cold stratospheric temperatures (*31–33*). Our results confirm that NAT particles exist in the atmosphere and are present in the north polar stratosphere, near or even above their equilibrium temperature. The complexity of particle occurrence, phase, and composition in the northern polar region has been known for some time (*1, 34*). Two flights of the ACMS have confirmed the existence of non-ice PSC particles by measurements of STS droplets in low-temperature PSCs in January 1998 (*14*) and NAT particles at higher temperatures in January 2000.

References and Notes

1. World Meteorological Organization (WMO), *Scientific Assessment of Ozone Depletion: 1998, Report 44* (Global Ozone Research and Monitoring Project, Geneva, 1999).
2. S. Solomon, *Rev. Geophys.* **37**, 275 (1999).
3. S. Pawson, B. Naujokat, *J. Geophys. Res* **104**, 14209 (1999).
4. L. R. Poole, M. P. McCormick, *Geophys. Res. Lett.* **15**, 21 (1988).
5. L. R. Poole, M. T. Osborn, W. H. Hunt, *Geophys. Res. Lett.* **15**, 867 (1988).
6. D. Fahey *et al.*, *J. Geophys. Res.* **94**, 11299 (1989).
7. P. J. Crutzen, F. Arnold, *Nature* **324**, 651 (1986).
8. O. B. Toon, P. Hamill, R. P. Turco, J. Pinto, *Geophys. Res. Lett.* **13**, 1284 (1986).
9. D. R. Hanson, K. Mauersberger, *Geophys. Res. Lett.* **15**, 855 (1988).
10. A. Tabazadeh, R. P. Turco, M. Z. Jacobson, *J. Geophys. Res.* **99**, 12897 (1994).
11. G. Beyerle, R. Neuber, O. Schrems, F. Wittrock, B. Knudsen, *Geophys. Res. Lett.* **21**, 57 (1994).
12. K. S. Carslaw *et al.*, *Geophys. Res. Lett.* **21**, 2479 (1994).
13. L. Iraci, A. T. J. Fortin, M. A. Tolbert, *J. Geophys. Res.* **103**, 8491 (1998).
14. J. Schreiner, C. Voigt, K. Mauersberger, F. Arnold, N. Larsen, *Science* **283**, 968 (1999).
15. N. Larsen *et al.*, *J. Geophys. Res.* **105**, 1491 (2000).
16. C. Voigt *et al.*, *Geophys. Res. Lett.*, in press.
17. J. Schreiner, U. Schild, C. Voigt, K. Mauersberger, *Aerosol Sci. Technol.* **31**, 373 (1999).
18. D. J. Hofmann, T. Deshler, *J. Geophys. Res.* **96**, 2897 (1991).
19. T. Deshler, S. J. Oltmans, *J. Atmos. Chem.* **30**, 11 (1998).
20. J. M. Rosen, N. T. Kjome, *Appl. Opt.* **30**, 1552 (1991).
21. A. Adriani *et al.*, in *Proceedings of XVIII Quadrennial Ozone Symposium, L'Aquila 1996, Atmospheric Ozone*, R. D. Bojkov, G. Visconti, Eds. (Edigrafital for Parco Scientifico e Tecnologico d'Abruzzo, L'Aquila, Italy, 1998), vol. 2, pp. 879–882.
22. J. Ovarlez, H. Ovarlez, *Geophys. Res. Lett.* **21**, 13, 1235 (1994).
23. A. Dörnbrack, M. Leutbecher, R. Kivi, E. Kyrö, *Tellus* **51A**, 951 (1999).
24. The mass spectrometer sensitivities for water and nitric acid have been calibrated through the introduction of known partial pressures of these substances into the particle evaporation sphere by means of a pressure-related dynamic expansion. The mole flux to the mass spectrometer can then be related to the count rate.
25. The selection of the integration period was guided by the measurements of the backscatter sondes and by the mass spectrometer signals of H_2O and HNO_3 (Fig. 2). The actual period selected for the integration is not very critical; for example, integration in a cloud layer for 100 s did not change the molar ratio beyond the uncertainties shown in Fig. 3. The beginning and the end of a cloud encounter were always well resolved.
26. The total particle volume was calculated from a bimodal log-normal fit to the particle size distribution measured with the particle counter. STS particles (e.g., centered around 75,100 s UT) resulted in distributions of particles with a median diameter of 0.14 μm (standard deviation $\sigma = 1.85$) and a number density of 15 cm^{-3} and, for the second mode, in diameters of 1.08 μm ($\sigma = 1.55$) and number density of 0.01 cm^{-3}. NAT particles (e.g., near 79,650 s UT) resulted in a median diameter of 0.13 μm ($\sigma = 1.50$) and a density of 16 cm^{-3} and in a diameter of 1.52 μm ($\sigma = 1.45$) and a density of 0.5 cm^{-3}.
27. Although no direct HNO_3 gas phase measurement was performed, a mixing ratio of 10 ppb is reasonable [S. Spreng, F. Arnold, *Geophys. Res. Lett.* **21**, 1251 (1994)]. Departures of 2.5 ppb will change T_{NAT} by less than 0.5 K.
28. One of us (N.L.) calculated the evaporation times of NAT particles assuming a 1 K temperature increase: The time for a 50% volume reduction is 2 hours for a particle of radius 1.0 μm, and 1 day for a particle of radius 5.0 μm.
29. R. Stolarski, *Nature* **389**, 788 (1997).
30. P. A. Newman, J. G. Gleason, R. D. McPeters, R. S. Solarski, *Geophys. Res. Lett.* **24**, 2689 (1997).
31. K. S. Carslaw *et al.*, *Nature* **391**, 675 (1998).
32. K. S. Carslaw *et al.*, *J. Geophys. Res.* **103**, 5785 (1998).
33. T. Deshler *et al.*, *J. Geophys. Res.* **105**, 3943 (2000).
34. T. Peter, *Annu. Rev. Phys. Chem.* **48**, 785 (1997).

35. The balloon flight was performed as part of the European-American THESEO-2000/SOLVE campaign in winter 1999/2000. The excellent support through the balloon launch team of the Centre National d'Etudes Spatiales (CNES) is acknowledged. Supported by the Commission of the European Union through the Environmental and Climate program (contract ENV4-CT97-0523) and by NSF grants OPP-9707520 and OPP-9423285 (T.D., C.K., and J.R.).

24 August 2000; accepted 26 October 2000

Reinterpreting Space, Time Lags, and Functional Responses in Ecological Models

Matt J. Keeling,[1]* Howard B. Wilson,[2] Steve W. Pacala[3]

Natural enemy-victim interactions are of major applied importance and of fundamental interest to ecologists. A key question is what stabilizes these interactions, allowing the long-term coexistence of the two species. Three main theoretical explanations have been proposed: behavioral responses, time-dependent factors such as delayed density dependence, and spatial heterogeneity. Here, using the powerful moment-closure technique, we show a fundamental equivalence between these three elements. Limited movement by organisms is a ubiquitous feature of ecological systems, allowing spatial structure to develop; we show that the effects of this can be naturally described in terms of time lags or within-generation functional responses.

Enemy-victim systems incorporate a large cross section of ecological interactions, including predator-prey, host-parasitoid, host-parasite, and host-pathogen systems. A number of important questions about these systems have emerged from both theoretical and empirical work over many decades. For example, given the inherent instabilities in the dynamics of such interactions, how do the species coexist? How do density dependence and the behavioral responses of the organisms influence the dynamics? What are the effects of limited movement in space, leading to noncomplete mixing? A unifying explanation or approach has re-

mained elusive, as it would seem that these are very distinct questions.

The theory of natural enemies developed under the assumption of homogeneity (*1–3*), which only holds for completely mixed populations, in which all the individuals experience the same environment. Although this has enabled the development of simple theory, real populations are always heterogeneous to some degree, and this has long been known to have a profound impact on the interactions between species (*4–8*). Even in situations where the external environment is uniform, modern analysis has shown that heterogeneities can be internally generated by the effects of limited movement and local interactions in space (*9–12*). A second form of heterogeneity, generated by stochastic events and individuality, has been increasingly regarded as also having a strong influence on large-scale ecological patterns (*13, 14*). However, because of the complexities inherent in stochastic spatial models, it has been difficult to combine these two elements and obtain rigorous insights.

Here we formulate fully analytical models for individual-based, stochastic metapopulations of the Nicholson-Bailey and Lotka-Volterra systems for natural enemies. This approach directly addresses the large population fluctuations that are due to discrete individuals and local environments, as well as the correlations that develop because of limited movement in space. When mixing is complete and all individuals disperse to other patches, then the organisms experience a uniform environment; however, with limited movement some individuals remain in a patch, causing correlations to rapidly develop. By assuming that the movement rates between patches are large but that complete mixing does not occur, we have gained spatial heterogeneity but are still able to formulate explicit models. These provide an intuitive understanding of how internally generated heterogeneity affects the dynamics of natural-enemy systems. Although our approximations are only rigorously valid when the movement rates are large, simulations have shown that the general results extend over a very wide range of movement rates and mixing levels.

Our individual-based Lotka-Volterra metapopulation model has local patch dynamics governed by the standard differential equations (*1, 2*), although because the model is individual-based, death, reproduction, and parasitism are now all stochastic events. In this metapopulation model, the local patches are linked by the random movement of individuals, where M_H and M_P are the rates at which hosts and parasites leave a patch, respectively. Dispersal is assumed to be global, so that an individual can disperse to any randomly selected patch. By considering the ensemble average (denoted by a bar) over a large number of patches and over all possible stochastic realizations, differential equations can be developed for any average quantity. The average numbers of hosts $\bar{H}_t$ and parasites $\bar{P}_t$ per patch at time t are described by

$$\frac{d\bar{H}_t}{dt} = r\bar{H}_t - \beta\overline{H_tP_t} = r\bar{H}_t - \beta\bar{H}_t\bar{P}_t - \beta\bar{C}_t$$

$$\frac{d\bar{P}_t}{dt} = \lambda\beta\overline{H_tP_t} - d\bar{P}_t = \lambda\beta\bar{H}_t\bar{P}_t - d\bar{P}_t + \lambda\beta\bar{C}_t$$

where r is the basic reproductive rate, β is the probability of hosts encountering parasites (the contact rate), λ is the mean brood size of the parasites, and $\bar{C}_t$ is the average covariance between numbers of hosts and parasites in a patch. These equations are exact and are equivalent to the standard Lotka-Volterra model (which has a single nontrivial, neutrally stable fixed point) except there is an additional term for the spatial covariance in the system.

Our other model, a discrete time system, can be viewed as either an adaptation of the continuous-time Lotka-Volterra equations or as a limiting case (where the parasitism function is linearized) of the Nicholson-Bailey model (*3*). In this system, there is a phase of reproduction and parasitism, which is then followed by a dispersal phase [as in (*12*)]; here m_H and m_P give the probability that a host or parasite (or parasitoid) leaves a patch during the dispersal phase. The equations for the change in the average number of hosts and parasites are

$$\bar{H}_{t+1} = F\bar{H}_t - aF\overline{H_tP_t} = F\bar{H}_t(1 - a\bar{P}_t) - aF\bar{C}_t$$

$$\bar{P}_{t+1} = a\overline{H_tP_t} = a\bar{H}_t\bar{P}_t + a\bar{C}_t$$

where F is the mean fecundity of the host (the number of progeny is assumed to be Poisson-distributed) and a is the probability that a parasite will find a given host within a patch. Again, these equations are exact, and errors only enter through our approximations for the covariance $\bar{C}_t$. The model is equivalent to the standard, linearized Nicholson-Bailey model (which has a single nontrivial but unstable fixed point) except that there is the additional term for the covariance.

The results of stochastic simulations of both the continuous and discrete time metapopulation models are shown in Fig. 1. Both systems show that limited movement can stabilize the dynamics—i.e., the system tends to spend more time closer to the fixed point and the persistence time of the populations is increased. (However, for some parameter choices the system can be destabilized). The change in stability comes from the buildup of correlations between hosts and natural enemies in the subpopulations. The presence of many parasites acts to drive down the number of hosts in that subpopulation, producing strong negative correlations, whereas the movement between patches acts to destroy these correlations. In the limit of complete mixing (when $M_H = M_P = \infty$ or $m_H = m_P =$

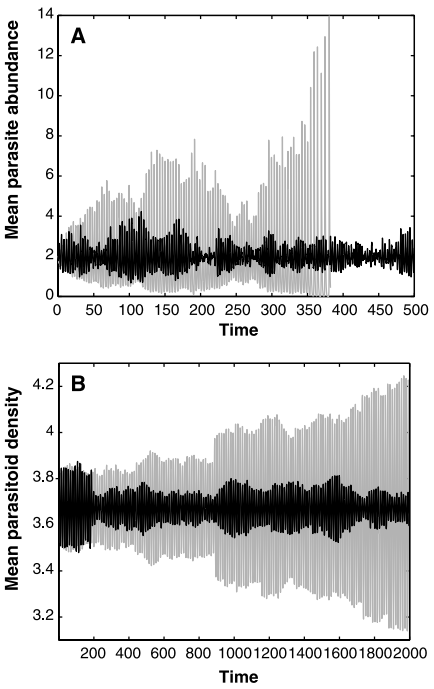

Fig. 1. Time series from the two stochastic systems, comparing the dynamics of a well-mixed (gray line) and a limited-movement (black line) model. (**A**) The individual-based Lotka-Volterra metapopulation. The black line is a typical simulation for $M_P = 13$ and $M_H = 2$. The gray line is a simulation at the Poisson limit $M_P, M_H \to \infty$, which shows greater deviations from the fixed point and is more prone to extinction. Interaction parameters are the same for both simulations ($r = 2$, $d = 1$, $\beta = 1$, and $\lambda = 1$) and the number of subpopulations is 500. (**B**) The individual-based Nicholson-Bailey metapopulation. The gray line is when $m_H = m_P = 1$ and the black line is when $m_H = m_P = 0.8$. To make the effects of decreasing movement probabilities more easily detectable, we modified the original equations so that the system is neutrally stable in the complete mixing limit ($m_H = m_P = 1$). This was achieved by introducing a carrying capacity for the hosts, so that $H_{t+1} = FH_t(1 - aP_t)(1 - H_t/K)$. Parameter values are $F = 1.5$, $a = 0.05$, and $K \approx 109$, and the number of subpopulations is one million.

[1]Department of Zoology, University of Cambridge, Downing Street, Cambridge CB2 3EJ, UK. [2]Department of Biology, Imperial College, Silwood Park, Ascot, Berkshire SL5 7PY, UK. [3]Department of Ecology and Evolutionary Biology, Princeton University, Princeton, NJ 08544–1003, USA.

*To whom correspondence should be addressed. E-mail: matt@zoo.cam.ac.uk

1), the correlations disappear, and the dynamics of the mean numbers of hosts and parasites is the same as for the nonspatial deterministic case. We seek to explain the change in the stability of these two natural-enemy systems as movement between patches decreases from this well-understood rapid-mixing limit.

Using moment-closure analysis (*15–18*) and treating the average covariance $\bar{C}$ as a separate variable, we find that for the continuous time model

$$\bar{C}_t \approx -\beta \int_0^\infty \exp(-(M_H + M_P)T) \times \bar{H}_{t-T}\,\bar{P}_{t-T}\,dT$$

Similarly, for the discrete time model

$$\bar{C}_t \approx -a^2F(1-m_H)(1-m_P)\bar{H}^2_{t-1}\,\bar{P}_{t-1}$$

These are first-order approximations to the average covariance $\bar{C}$ and assume that there is a large amount of movement between subpopulations, so that variances and higher order cumulants can be approximated by their Poisson limits (*18*). These covariances can be viewed in three distinct ways.

First, the covariance can be interpreted as an extra dimension, informing us about the spatial arrangement of species. In this role, we find that as $\bar{C}$ is always negative, so hosts and parasites are more likely to occupy distinct patches than their mean abundances would predict.

Second, because the covariance in both systems is dependent only on the mean number of hosts and parasites in the past, an alternative approach would be to include the covariance as a time delay in the models, so that both the present and previous means have an impact on the future: the system has a "spatial memory." When movement between patches is rapid, the spatial memory is destroyed very quickly; hence, only a first-order time lag is needed. However, when the movement is reduced, the effects of local interactions take longer to diffuse into the population; in the equations this corresponds to reduced accuracy of our first-order approximations. To obtain second-order approximations requires either an extra time lag or an extra set of moments (including variances and some third-order cumulants). This formulation can be compared to work with embedding dimensions (*19*), where it is a general result that extra (lagged) information may be used to capture the dynamics of a spatial system (*20*). The reformulation given here explicitly creates the required form of the time lag and shows that the length and time scale of this lagged information, and hence the complexity of the dynamics, increase as the level of spatial mixing decreases. In this system and in many other natural enemy models, the time lags obtained take on the form of delayed density dependence and, as such, provide a useful representation of spatial heterogeneity when the number of lags needed is small.

Third, for the discrete time model, because the particular map is invertible (except when H or P is zero), it is possible to express the means one time step ago in terms of the current species levels, hence

$$\bar{C}_t \approx -a(1-m_H)(1-m_P)\bar{P}_t(\bar{H}_t + F\bar{P}_t)$$

This expression for the covariance may be substituted into the two difference equations, where it acts as a functional response. This can be compared to previous host-parasitoid models in which a modified functional response has been used to mimic the effects of spatial clustering (*5, 21*). It should be realized that, because all maps are not necessarily invertible, this step cannot always be accomplished. Here, the correlation term reduces the host risk of parasitism and decreases the parasite success rate as the number of parasitoids per host increases; it is therefore analogous to competition between parasitoids.

Thus, the spatial structure represented by $\bar{C}$ (the average covariance in the abundances of hosts and parasites) can also be interpreted either as a time-lagged density-dependent effect or, for the discrete time model, as a more complex functional response, which reduces the effectiveness of the parasites at high parasite density.

To first order, the negative correlation is found to have a stabilizing effect on the dynamics of the discrete time model, although the effect is never strong enough to fully stabilize the fixed point. Numerical simulations of the full stochastic system, however, indicate that when the movement probabilities are lower, higher order effects may be sufficient to stabilize the dynamics. Figure 2A shows two distinct regimes where persistence times are large, which correspond to where heterogeneity in host or parasite abundances is high (*22*). For the continuous time system, the movement rates control both the magnitude and mean duration of the time lag, resulting in an exponentially decaying lag that has no stability effects to first order. However, at second order, this Lotka-Volterra system can be either stabilized or destabilized, depending on the relative magnitudes of the host and parasite movements. In the stochastic simulations where the effects of all orders are incorporated, the populations show the greatest persistence when one of the movement rates is small; however, if both rates are small, then extinctions become far more common (Fig. 2B). The persistence results of both simulations agree well with the stability analysis of the moment-closure equations (*18*), with long persistence times corresponding to greater stability of the fixed point.

A growing number of examples of delayed density dependence (DDD) have been detected in field populations, most frequently in forest insects and small mammals (*23–26*). Numerous mechanisms have been proposed to explain these delay effects, with the most frequent being trophic interactions. Because limited movement is a ubiquitous feature of ecological systems, it may prove to be important in understanding how density dependence operates in such systems. The precise effects on stability, however, depend on the precise details of the underlying biology (*27, 28*).

We believe that the interpretation of spatial heterogeneity in terms of time lags and functional responses is generic, because similar techniques could be applied to any equations describing an ecological system. This

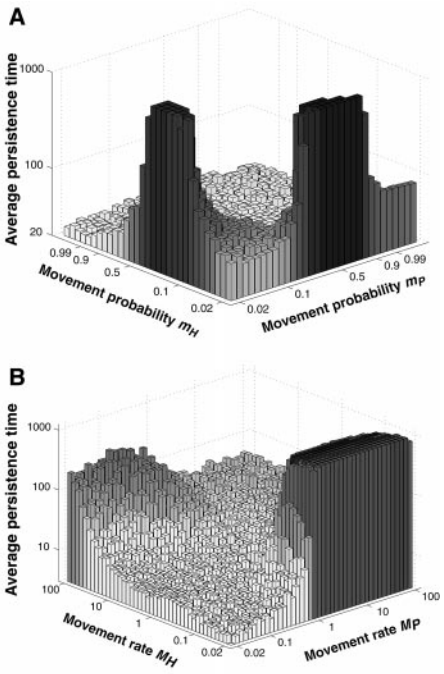

Fig. 2. Graphs showing the persistence times from stochastic simulations of the two systems; the shading becomes darker as the persistence times increase. The movement terms from the two models can be linked by considering the probability that an individual in the Lotka-Volterra system leaves a patch during one unit of time: $Prob(\text{leaving}) = 1 - exp(-M)$. The two graphs are therefore at similar scales. (**A**) The Nicholson-Bailey metapopulation. Each persistence time is an average of five independent simulations, where the maximum time is 1000 generations ($F = 1.5$, $a = 0.1$) and the number of subpopulations is 2500. (**B**) The Lotka-Volterra metapopulation. The persistence time is a smoothed average of five independent simulations, where the maximum time was set at 1000. The number of subpopulations is 500 ($r = 1$, $d = 1$, $\beta = 1$, and $\lambda = 1$).

equivalence should facilitate a more unified approach in understanding all natural enemy-victim interactions. Interpreting spatial heterogeneity in terms of time delays is likely to be a powerful tool for understanding many complex ecological situations. Not only have more statistical tools and more biological intuition been developed to deal with DDD, but in general the data needed to study temporal lags are far more readily attainable than the data needed to study spatial structure.

References and Notes

1. A. J. Lotka, *The Elements of Physical Biology* (Williams & Williams, Baltimore, MD, 1925).
2. V. Volterra, *Nature* **118**, 558 (1926).
3. A. J. Nicholson, V. A. Bailey, *Proc. Zool. Soc. London* **3**, 551 (1935).
4. C. B. Huffaker, *Hilgardia* **27**, 343 (1958).
5. M. P. Hassell, R. M. May, *J. Anim. Ecol.* **43**, 567 (1974).
6. A. Hastings, *Theor. Popul. Biol.* **12**, 37 (1977).
7. R. M. May, *J. Anim. Ecol.* **47**, 833 (1978).
8. I. Hanski, *Ecology* **64**, 493 (1983).
9. P. Kareiva, *Philos. Trans. R. Soc. London Ser. B* **330**, 175 (1990).
10. R. Durrett, S. A. Levin, *Theor. Popul. Biol.* **46**, 363 (1994).
11. M. Keeling, in *Advanced Ecological Theory*, J. McGlade, Ed. (Blackwell Science, Oxford, 1999), pp. 64–99.
12. M. P. Hassell, H. Comins, R. M. May, *Nature* **353**, 255 (1991).
13. E. McCauley, W. G. Wilson, A. M. DeRoos, *Am. Nat.* **142**, 412 (1993).
14. S. W. Pacala *et al.*, *Ecol. Monogr.*, **66**, 1 (1996).
15. E. Renshaw, *Modelling Biological Populations in Space and Time* (Cambridge Univ. Press, Cambridge, 1991).
16. M. Keeling, *J. Anim. Ecol.* **69** 725 (2000).
17. B. M. Bolker, S. W. Pacala, *Am. Nat.* **153**, 575 (1999).
18. The full equations for the numbers of hosts (H) and parasites (or parasitoids) (P) clearly depend on a higher moment, namely the average covariance $\bar{C}_t$. By considering all stochastic events that can occur, we can also formulate an equation describing the dynamics of $\bar{C}_t$; however, this will also include higher moments. The moment closure analysis approximates these higher moments by their equivalent values for a Poisson distribution. When the movement rates are large, the effect of this Poisson assumption on the covariance is small and the corresponding effects on the mean number of H and P is smaller still. Extensive simulations have shown that approximations of this order are still valid even when the movement rates are quite small. The full derivation of the equations and stability analysis is given in the supplementary Web material (*29*).
19. D. S. Broomhead, G. P. King, *Physica D* **20**, 217 (1986).
20. H. B. Wilson, D. A. Rand, *Proc. R. Soc. London Ser. B* **264**, 625 (1997).
21. M. P. Hassell, *The Dynamics of Arthropod Predator-Prey Systems* (Princeton Univ. Press, Princeton, NJ, 1978).
22. S. W. Pacala, M. P. Hassell, *Am. Nat.* **138**, 584 (1991).
23. P. Turchin, *Nature* **344**, 660 (1990).
24. B. Hornfeldt, *Ecology* **75**, 791 (1994).
25. O. N. Bjornstad *et al.*, *J. Anim. Ecol.* **67**, 110 (1998).
26. T. Saitoh, N. C. Stenseth, O. N. Bjornstad, *Res. Popul. Ecol.* **40**, 61 (1998).
27. E. E. Crone, *Theor. Popul. Biol.* **51**, 67 (1997).
28. D. J. Rodriguez, *J. Theor. Biol.* **191**, 95 (1998).
29. Available on *Science* Online at www.sciencemag.org/cgi/content/full/290/5497/1758/DC1

30. We thank M. Hassell for his valuable comments on the manuscript. M.J.K. is supported by a Royal Society University Training Fellowship. H.B.W. is supported by a National Environment Research Council Advanced Fellowship.

16 August 2000; accepted 11 October 2000

Posttranslational N-Myristoylation of BID as a Molecular Switch for Targeting Mitochondria and Apoptosis

Jiping Zha,* Solly Weiler,* Kyoung Joon Oh, Michael C. Wei, Stanley J. Korsmeyer†

Many apoptotic molecules relocate subcellularly in cells undergoing apoptosis. The pro-apoptotic protein BID underwent posttranslational (rather than classic cotranslational) N-myristoylation when cleavage by caspase 8 caused exposure of a glycine residue. N-myristoylation enabled the targeting of a complex of p7 and myristoylated p15 fragments of BID to artificial membranes bearing the lipid composition of mitochondria, as well as to intact mitochondria. This post-proteolytic N-myristoylation serves as an activating switch, enhancing BID-induced release of cytochrome c and cell death.

Localization of proteins to distinct subcellular compartments, including membranes, is a critical event in multiple cellular pathways such as apoptosis. Discrete topogenic sequence elements within proteins function as an address for unidirectional targeting to select membrane sites (*1*). Alternatively, lipid modification of proteins, including isoprenylation, myristoylation, palmitoylation, or modification by glycosyl-phosphatidylinositol, enables targeting and permits stable membrane association (*2*, *3*). One drastic cell fate decision, apoptosis, follows signal transduction events and results in the redistribution of proteins, which often initiates their effector activity. Phosphorylation, a well-documented mechanism that can relocate proteins (*4*), regulates the movement of pro-apoptotic BAD from cytosol to mitochondria (*5*) and the movement of Forkhead transcription factor (FKHRL1) from cytosol to nucleus (*6*). In *Caenorhabditis elegans*, the pro-apoptotic molecule Egl-1 releases Ced-4 from mitochondria, which then travels to nuclear membranes (*7*). Site-specific cleavage of several hundred death substrates by dedicated proteases, called caspases, is a critical step in the execution phase of apoptosis (*8*). For example, cleavage of the chaperone ICAD releases its partner CAD (caspase-activated deoxyribonuclease), which translocates to the nucleus to degrade DNA (*9*, *10*). Other caspase substrates include DNA repair enzymes, structural components of the cytoskeleton or nuclear scaffold, and BCL-2 family proteins that affect mitochondrial dysfunction (*8*, *11–14*). This includes the pro-apoptotic molecule BID, a member of the "BH3 domain only" subset that links proximal signals from death receptors to the common apoptotic pathway (*11–13*). Engagement of the receptor Fas (CD95) or of tumor necrosis factor receptor 1 (TNFR1) activates caspase 8, which cleaves the inactive cytosolic form of BID (p22), generating a truncated 15-kd fragment (tBID) (*11–13*) that relocates to mitochondria within 1 hour. The exposed BH3 domain of tBID (*15*, *16*) binds and oligomerizes BAK, a resident mitochondrial family member with multiple BH domains, resulting in mitochondrial dysfunction, including the release of cytochrome c (*17*). How BID rapidly and selectively targets the mitochondrial outer membrane remains unresolved.

Multidimensional nuclear magnetic resonance analysis indicated that uncleaved and cleaved BID have approximately the same conformation in solution, suggesting that the p7 and p15 fragments remain in a noncovalent complex after cleavage by caspase 8 (*15*). Consequently, we explored the mechanism by which this complex translocated to and inserted into the mitochondrial membrane. We confirmed that the p15 tBID fragment was not released when recombinant full-length p22 was cleaved by caspase 8. When NH_2-terminal histidine-tagged p7 (his-p7) was released from a nickel agarose column by imidazole, the p15 tBID fragment always coeluted (Fig. 1A, lane 1), suggesting a tight noncovalent complex. The solution structure of p22 BID suggests that a hydrophobic interaction between α1 and α3 helices may be responsible (*15*, *16*). In support of this idea, p15 was only dissociated from his-p7 when the nonionic detergent *n*-octyl glucoside reached its critical micelle concentration (0.6% w/v), indicating a strong hydrophobic interaction (Fig. 1A) (*15*, *18*). We

Howard Hughes Medical Institute, Dana-Farber Cancer Institute, Departments of Pathology and Medicine, Harvard Medical School, Boston, MA 02115, USA.

*These authors contributed equally to this work.
†To whom correspondence should be addressed. E-mail: stanley_korsmeyer@dfci.harvard.edu